Fast simulations with high accuracy for photonic crystals and quantum nanostructures enabled by a projection-based learning methodology

Martin Veresko^a, Albert WB Wang^{b,c}, Ming-Cheng Cheng*,^a

^aDept. of Electrical and Computer Engineering, Clarkson University, Potsdam, NY 13699-5720

^bDept. of Physics and Astronomy, Bates College, Lewiston, Maine 04240

^cCurrent Affiliation: Dept. of Electrical Engineering, Columbia University, New York, NY 10027

ABSTRACT

A fast and accurate simulation methodology enabled by a physics-informed learning method, using proper orthogonal decomposition (POD) and Galerkin projection, is demonstrated for photonic crystals and periodic quantum nanostructure. POD is a projection-based method with its basis functions trained by solution data collected from direct numerical simulations (DNSs) of the wave equation, which offers the best least squares fit to the solution data. The Galerkin projection of the wave equation onto POD basis functions is then performed to close the model. This projection also incorporates physical principles during POD-Galerkin simulation guided by the wave equation, which thus enables the extrapolation capability beyond the training conditions. Such a capability is difficult to achieve using neural-network-based methods for physics simulation, where no physical principle is enforced during simulation. Applications of the POD-Galerkin methodology to a 2D photonic lattice and a 2D periodic quantum nanostructure demonstrate a computing speedup near 2 orders of magnitude with high accuracy, compared to DNS, if the wave solution and band structure are both needed. If only the band structure is of interest, a 4-order improvement in computational efficiency can be achieved.

Keywords: Physics-informed leaning, photonic crystals, electronic superlattices, POD, Galerkin projection, electronic band structure, optical band structure

1. INTRODUCTION

A wide range of science and engineering applications for materials, devices and systems utilizing electronic and optical properties resulting from periodic quantum nanostructures and photonic crystals, respectively [1-7]. Design and analysis of periodic electronic nanostructures or photonic crystals for various applications in general require solutions of eigenvalue problems involving the Schrödinger equation and/or electromagnetic wave equation. For simple periodic structures, wave solutions may be obtained from analytical, transmission-line, scattering-matrix and/or transfer-matrix methods [8-13]. If one desires high accuracy in simulations of electronic or optical superlattices involving complex multi-dimensional structures, computationally intensive direct numerical simulations (DNSs) with fine spatial resolution are always needed.

Another popular method for periodic structures involves a projection-based approach using the Fourier plane-wave expansion due to the periodic nature of the Fourier basis. It has been shown in previous work that the assumed Fourier plane-wave method converges slowly for a complex periodic structure [14]. The current work investigates an effective simulation methodology enabled by a learning algorithm based on proper orthogonal decomposition (POD) [15], together with Galerkin projection [14-19]. POD is also a projection-based method with its basis functions (hereafter named POD modes) optimized by a training process via solution data. To generate optimal modes, training data are collected from DNSs subjected to parametric variations for the problem of interest, instead of adopting an assumed basis set, such as Fourier, Legendre, Bessel, Wannier and Airy functions. Each set of these assumed basis functions is valid only for a specific type of problems. To close the POD data-learning simulation model, Galerkin projection of the wave equation onto each of the trained POD modes is carried out. Such a rigorous procedure for deriving the POD-Galerkin model ensures that (i) the generated modes are optimized and tailored to the parametric variations in the system of interest with a best least squares (LS) fit to information embedded in the training data and (ii) physical principles guided by the wave equation

^{*} Corresponding author: mcheng@clarkson.edu

are appropriately accounted for in the developed model. This is very different from some deep learning methods using physics-informed neural networks (PINNs) where physical principles are enforced only during the training process [20-22]. On the contrary, the POD-Galerkin method imposes physical principles for every single calculation during the prediction/simulation enabled by the Galerkin projection of the governing equation. As a result, the POD-Galerkin simulation methodology offers not only accurate and efficient solution of the problem but also a remarkable extrapolation and learning abilities [14, 16, 19]. These abilities will be presented in this work for wave solutions and band structures in photonic crystals and periodic quantum nanostructures.

2. POD-GALERKIN FOR WAVE EQUATION IN PERIODIC STRUCTURES

Wave solution in a periodic lattice structure can be represented by a Bloch function, described by a periodic function $u_{\mathbf{k}}(\mathbf{r})$ modulated by a plane wave,

$$w_{\mathbf{k}}(\mathbf{r}) = e^{i\mathbf{k}\cdot\mathbf{r}}u_{\mathbf{k}}(\mathbf{r}),\tag{1}$$

where $u_{\mathbf{k}}(\mathbf{r})$ has the same periodicity as the lattice and \mathbf{k} is the wave vector. Applying the wave equation for $w_{\mathbf{k}}(\mathbf{r})$ to the Bloch function in (1), a wave equation for $u_{\mathbf{k}}(\mathbf{r})$ can be derived, which is briefly presented below for periodic nanostructures and photonic crystals.

Periodic quantum nanostructures

In electronic superlattices, the electron wave function (WF) $\psi_{\bf k}({\bf r})$ is described by the Schrodinger equation,

$$\nabla \cdot \left[-\frac{\hbar^2}{2m^*} \nabla \psi_{\mathbf{k}} \right] + U(\mathbf{r}) \psi_{\mathbf{k}} = \mathcal{E}_{\mathbf{k}} \psi_{\mathbf{k}}, \tag{2}$$

where \hbar is the reduced plank constant, m^* the effective mass, $U(\mathbf{r})$ the potential energy, and $\mathcal{E}_{\mathbf{k}}$ the eigenstate energy of the electron with momentum of $\hbar \mathbf{k}$. Using (1) for $\psi_{\mathbf{k}}$ in (2), the effective Schrodinger equation for the \mathbf{k} -state WF $u_{\mathbf{k}}(\mathbf{r})$ can be derived as,

$$-\nabla \cdot \frac{\hbar^2}{2m^*} \nabla u_{\mathbf{k}} - i\mathbf{k} \cdot \left[\frac{\hbar^2}{2m^*} \nabla u_{\mathbf{k}} + \nabla \frac{\hbar^2 u_{\mathbf{k}}}{m^*} \right] + \frac{\hbar^2 k^2}{2m^*} u_{\mathbf{k}} + U u_{\mathbf{k}} = \mathcal{E}_{\mathbf{k}} u_{\mathbf{k}}. \tag{3}$$

For a free electron in a periodic structure, (3) is reduced to

$$\left[\frac{\hbar^2}{2m_o}(-i\nabla + \mathbf{k})^2 + U\right]u_{\mathbf{k}} = \mathcal{E}_{\mathbf{k}}u_{\mathbf{k}},\tag{4}$$

where m_o the free electron mass.

Photonic crystals

Considering the TE mode for 2D photonic crystals, electric field $E_{z,k}$ perpendicular to the 2D surface is described by the Helmholtz Equation,

$$\nabla^2 E_{z,\mathbf{k}} = -\left(\frac{\omega_{\mathbf{k}}}{c}\right)^2 \epsilon_r E_{z,\mathbf{k}},\tag{5}$$

where $\omega_{\mathbf{k}}$ is the harmonic angular frequency, c is the speed of light and ϵ_r is the relative permittivity. Using the Bloch function for $E_{z,\mathbf{k}}$ in (1), the wave equation for the periodic function $u_{\mathbf{k}}(\mathbf{r})$ can be derived from (5),

$$\left(\frac{\nabla + i\mathbf{k}}{\sqrt{\epsilon_r}}\right)^2 u_{\mathbf{k}} = -\left(\frac{\omega_{\mathbf{k}}}{c}\right)^2 u_{\mathbf{k}}.\tag{6}$$

To construct a POD-Galerkin simulation model, one can collect solution data of $u_{\mathbf{k}}(\mathbf{r})$ from DNSs of the wave equation given in (4) or (6) for a quantum nanostructure or photonic crystal, respectively. With generated POD modes from the data, the Galerkin projection of the wave equation onto the generated modes is then performed to close the model. The mode training and Galerkin projection are presented below.

2.1 Fundamentals of POD

Using the projection-based approach for a periodic structure, solution of $u_{\mathbf{k}}(\mathbf{r})$ can be expressed by a linear combination of a finite set of basic functions $\eta_{\mathbf{k}}(\vec{r})$,

$$u_{\mathbf{k}}(\mathbf{r}) = \sum_{n=1}^{M} a_{\mathbf{k},n} \eta_{\mathbf{k},n}(\mathbf{r}), \qquad (7)$$

where M is the selected number of basis functions (modes) or the degrees of freedom (DoF) to represent the solution, and $a_{\mathbf{k},n}$ is the weighting coefficient for $\eta_{\mathbf{k},n}$. The selection of the basis is not unique; however, it is of best interest to utilize the basis functions that offer the best fit to the solution.

POD trains an optimal set of modes to acquire essential information embedded in the collected data to offer the best LS fit to the solution using the smallest number of modes. This is achieved by maximizing the mean square of the solution projection in the entire simulation domain onto each of the modes $\eta_{\mathbf{k}}(\vec{r})$ over multiple samples of solution data for the problem of interest. That is,

$$\max_{\eta_{\mathbf{k}}} \frac{\langle |u_{\mathbf{k}} \cdot \eta_{\mathbf{k}}|^2 \rangle}{|\eta_{\mathbf{k}}|^2},\tag{8}$$

where the brackets $\langle \rangle$ denote the average over multiple samples of solution data with the inner product given as

$$u_{\mathbf{k}} \cdot \eta_{\mathbf{k}} = \int_{\Omega} u_{\mathbf{k}}^*(\mathbf{r}) \eta_{\mathbf{k}}(\mathbf{r}) d\Omega, \qquad (9)$$

and the L2 norm of $\eta_{\mathbf{k}}$ expressed as

$$|\eta_{\mathbf{k}}| = \sqrt{\int_{\Omega} |\eta_{\mathbf{k}}(\mathbf{r})|^2 d\Omega}.$$
 (10)

The solution data are collected from DNSs of the governing equation for the problem, accounting for parametric variations of the system, including boundary conditions (BCs). This process ensures that the modes $\eta_{\mathbf{k}}(\mathbf{r})$ contain the maximum LS information of the system embedded in the collected training data. Using variational calculus, (8) leads to an eigenvalue problem for the spatial autocorrelation function $\mathbf{R}(\mathbf{r}, \mathbf{r}')$ of the training data,

$$\int_{\Omega'} \mathbf{R}_{\mathbf{k}}(\mathbf{r}, \mathbf{r}') \eta_{\mathbf{k}}(\mathbf{r}') d\Omega' = \lambda_{\mathbf{k}} \eta_{\mathbf{k}}(\mathbf{r}), \qquad (11)$$

where $\lambda_{\mathbf{k}}$ is the POD eigenvalue and $\mathbf{R}_{\mathbf{k}}(\mathbf{r}, \mathbf{r}')$ is given by

$$R_{\mathbf{k}}(\mathbf{r}, \mathbf{r}') = \langle u_{\mathbf{k}}(\mathbf{r}) \otimes u_{\mathbf{k}}(\mathbf{r}') \rangle. \tag{12}$$

 $\lambda_{\bf k}$ represents the mean squared solution captured by each mode over the entire domain at each ${\bf k}$.

To efficiently solve the large-scale eigenvalue problem for a multi-dimensional domain, the method of snapshots [23, 24] is applied. Using the snapshot method, the eigenvalue problem in (11) in a discrete spatial domain with a dimension of $N_r \times N_r$ is converted to a sampling domain with a dimension of $N_s \times N_s$, where N_r and N_s are the numbers of spatial grid points and data samples (or snapshots), respectively, and in general $N_s << N_r$. When using equal spatial divisions in DNSs to collect training data, the method of snapshots can be simply applied via the singular decomposition (SVD). However, with unequal divisions, unequal weightings for individual meshes needed to be accounted for through integrals of the data, which is detailed in [24]. Instead of the N_r eigenvalues given in (11), the snapshot method solves only the first N_s POD eigenvalues and modes. The number of data samples thus needs to be large enough to ensure that $N_s > M$, where M is the number of modes used to represent the solution, and $\lambda_{\mathbf{k},M}$ should be many orders smaller than $\lambda_{\mathbf{k},1}$ to minimize the numerical error resulting from the POD prediction.

2.2 Galerkin projection

Formulations for Galerkin projections of (3) and (6) for $u_{\mathbf{k}}(\mathbf{r})$ in periodic quantum nanostructure and photonic crystals, respectively, are presented below.

Periodic quantum nanostructures

To close the POD-Galerkin model for solving u_k in (7) for the electron WF $u_k(\mathbf{r})$, (3) is projected onto the generated POD modes based on Galerkin projection and can be shown as,

$$k^{2} \int_{\Omega} \eta_{\mathbf{k},m}^{*} \frac{\hbar^{2} u_{\mathbf{k}}}{2m^{*}} d\Omega + \int_{\Omega} \nabla \eta_{\mathbf{k},m}^{*} \cdot \frac{\hbar^{2}}{2m^{*}} \nabla u_{\mathbf{k}} d\Omega - i\hbar \mathbf{k} \cdot \int_{\Omega} \eta_{\mathbf{k},m}^{*} \left(\frac{\hbar}{2m^{*}} \nabla u_{\mathbf{k}} + \hbar \nabla \frac{u_{\mathbf{k}}}{2m^{*}} \right) d\Omega - \int_{\Gamma} \eta_{\mathbf{k},m}^{*} \frac{\hbar^{2}}{2m^{*}} \nabla u_{\mathbf{k}} \cdot d\mathbf{S} + \int_{\Omega} \eta_{\mathbf{k},m}^{*} U u_{\mathbf{k}} d\Omega = \mathcal{E}_{\mathbf{k}} \int_{\Omega} \eta_{\mathbf{k},m}^{*} u_{\mathbf{k}} d\Omega.$$

$$(13)$$

Using (7), a matrix eigenvalue equation in the POD space for $a_{k,m}$ can be derived,

$$\sum_{n=1}^{M} (T_{m,n} + U_{m,n} + B_{m,n}) a_{k,n} = \mathcal{E}_{k} a_{k,m}, \quad \text{for } m = 1 \text{ to } M$$
 (14)

where Hamiltonian in the POD space includes interior kinetic $(T_{m,n})$, potential $(U_{m,n})$ and boundary kinetic $(B_{m,n})$ energy, and they are defined as follows,

$$T_{m,n} = \int_{\Omega} \left[\eta_{\mathbf{k},m}^* \frac{\hbar^2 k^2}{2m^*} \eta_{\mathbf{k},n} + \nabla \eta_{\mathbf{k},m}^* \cdot \frac{\hbar^2}{2m^*} \nabla \eta_{\mathbf{k},n} - i\hbar \mathbf{k} \cdot \eta_{\mathbf{k},m}^* \left(\frac{\hbar}{2m^*} \nabla \eta_{\mathbf{k},n} + \hbar \nabla \frac{\eta_{\mathbf{k},n}}{2m^*} \right) \right] d\Omega, \tag{15}$$

$$U_{m,n} = \int_{\Omega} \eta_{\mathbf{k},m}^* U \eta_{\mathbf{k},n} d\Omega \,, \tag{16}$$

$$B_{m,n} = \int_{\mathbf{S}} \eta_{\mathbf{k},m}^* \frac{\hbar^2}{2m^*} \nabla \eta_{\mathbf{k},n} \cdot d\mathbf{S} , \qquad (17)$$

Photonic crystals

Similarly to the quantum problem, to solve the weighting coefficients of POD modes for u_k in (7) for photonic crystals, the Galerkin projection of (6) onto the POD space is performed,

$$k^{2} \int_{\Omega} \frac{\eta_{\mathbf{k},m}^{*}}{\epsilon_{r}} u_{\mathbf{k}} d\Omega - 2i\mathbf{k} \cdot \int_{\Omega} \frac{\eta_{\mathbf{k},m}^{*}}{\epsilon_{r}} \nabla u_{\mathbf{k}} d\Omega + \int_{\Omega} \nabla \frac{\eta_{\mathbf{k},m}^{*}}{\epsilon_{r}} \cdot \nabla u_{\mathbf{k}} d\Omega - \int_{\Omega} \frac{\eta_{\mathbf{k},m}^{*}}{\epsilon_{r}} \nabla u_{\mathbf{k}} \cdot d\mathbf{S} = \left(\frac{\omega_{\mathbf{k}}}{c}\right)^{2} \int_{\Omega} \eta_{\mathbf{k},m}^{*} u_{\mathbf{k}} d\Omega.$$
 (18)

Using (7), (18) become a matrix eigenvalue equation,

$$\sum_{n=1}^{M} \left(T_{m,n} + B_{m,n} \right) a_{\mathbf{k},n} = \left(\frac{\omega_{\mathbf{k}}}{c} \right)^2 a_{\mathbf{k},m}, \quad \text{for } m = 1 \text{ to } M$$
 (19)

where

$$T_{m,n} = \int_{\Omega} \left(k^2 \frac{\eta_{\mathbf{k},m}^*}{\epsilon_r} \eta_{\mathbf{k},n} + \nabla \frac{\eta_{\mathbf{k},m}^*}{\epsilon_r} \cdot \nabla \eta_{\mathbf{k},n} - 2i\mathbf{k} \cdot \frac{\eta_{\mathbf{k},m}^*}{\epsilon_r} \nabla \eta_{\mathbf{k},n} \right) d\Omega, \tag{20}$$

$$B_{m,n} = \int_{S} \frac{\eta_{\mathbf{k},m}^{*}}{\epsilon_{r}} \nabla \eta_{\mathbf{k},n} \cdot d\mathbf{S}.$$
 (21)

Once POD modes are generated from the collected solution data for $u_{\mathbf{k}}(\mathbf{r})$, the matrix elements given in (15)-(17) for periodic quantum nanostructures or (20) and (21) for photonic crystals can be evaluated for $\mathbf{a} = [a_1, a_2, ..., a_n, ..., a_M]^T$.

3. VALIDATION OF POD-GALERKIN SIMULATION METHODOLOGY

The proposed POD-Galerkin methodology is validated in several electronic and optical structures in this work. To construct a POD-Galerkin model, POD modes need to be generated via training data accounting for variations of system parameters. For the electronic nanostructure, POD modes are trained by data of the \mathbf{k} -state WF $u_{\mathbf{k}}$ in (3) collected from DNSs subjected to variation of applied electric field in x and periodic BCs in y. For photonic crystals, modes are trained by electric field data of $u_{\mathbf{k}}$ in (6) via DSNs subjected to periodic BCs and variation of refractive indices of the materials. For either electronic or optical structure, the training is first presented below, followed by a demonstration of the POD-Galerkin methodology. The learning ability of the methodology is also demonstrated in situations within and beyond the training bounds.

3.1 Demonstrations in a 2D periodic quantum nanostructure

A 2D quantum dot (QD) structure is constructed by periodic GaAs/InAs given in Fig. 1(a) with periods of 7 nm and 6.3 nm in the x and y directions, respectively. The band offset is $\Delta E = 0.544 \, \mathrm{eV}$ and effective masses are $m_{GaAs}^* = 0.067 m_o$ and $m_{InAs}^* = 0.023 m_o$. Training data for $u_{\mathbf{k}}(\mathbf{r})$ are collected from DNSs of (3) for the QD structure, and the method of snapshots [23, 24] is applied to generate POD modes. In DNSs, a periodic BC is implemented in y, and 10 electric fields evenly spaced from 0 to 30kV/cm are applied in x with homogeneous BCs on both ends. The DNSs collect the data for $u_{\mathbf{k}}(\mathbf{r})$ in each \mathbf{k} state for the first 8 quantum states. There are thus 80 sets of solution data to generate one set of POD modes for each \mathbf{k} point in the Brillouin zone, accounting for field variation in x. The model parameters given by (15)-(17) are then evaluated using the generated modes for the matrix eigenvalue equation in (14). The electronic band structure for the periodic QD structure is thus determined in the Brillouin zone once a and a0 and a1 are solved from (14) and post processing via (7) can be used to calculate a1.

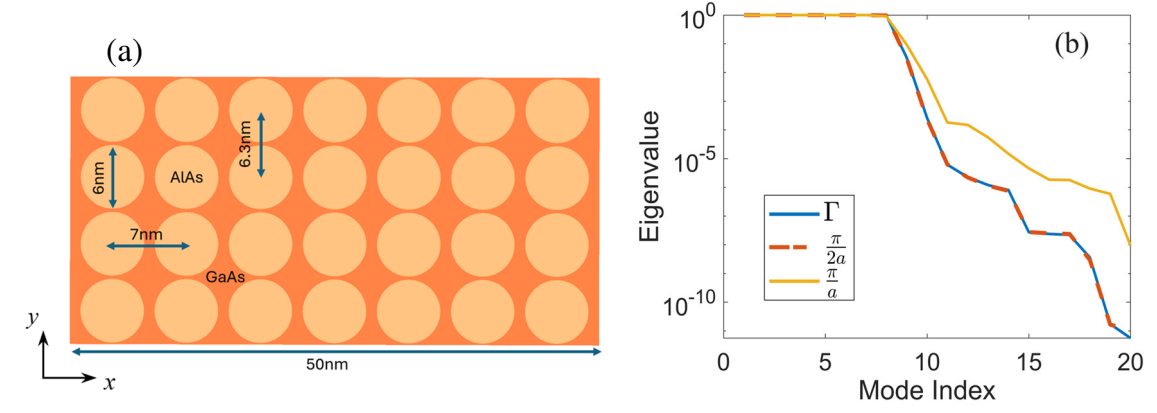


Figure 1. (a) 2D periodic GaAs/AlAs QD structure. (b) POD eigenvalues in descending order at the Γ point and $k = \pi/2a$ and π/a .

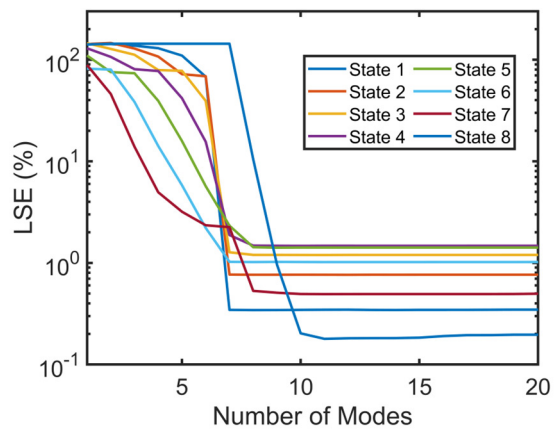


Figure 2. Relative LSE for the first 8 quantum states with respect to the DNS results at $k = \pi/2a$.

The POD eigenvalue spectrums for several **k** points in the Brillouin zone are illustrated in Fig. 1(b). The fast-declining eigenvalue implies that an accurate prediction can be achieved by POD-Galerkin using a small number of modes if the quality of training data is sufficient. For the first validation, electric field at 20kV/cm different from any field used in the training is applied in x to the QD structure. As shown in Fig. 2 at $k = \pi/2a$, the LSE of the periodic WF compared to the DNS solution in each quantum state resulting from POD-Galerkin varies significantly. All WFs at $k = \pi/2a$ reach an LSE lower than 1.43% with 7 or 8 modes except for State 8 whose LSE is near 10.5% with 8 modes but reduces to 0.96% and 0.2% with 9 or 10 modes, respectively. States 1, 2, 6 and 7 also achieve an LSE near or below 1% when using 7 or 8 modes. The profiles of $|u_{\mathbf{k}}(\mathbf{r})|^2$ along the field direction through the maximum value of $|u_{\mathbf{k}}(\mathbf{r})|^2$ is illustrated in Fig. 3 for several quantum states using one to 7 or 8 modes and they appear to nearly overlap with those from DNSs. Fig. 4(a) also illustrates that POD-Galerkin and DNS agree very well with each other for the prediction of the electronic band structure and their results are nearly identical. The larger errors shown in Fig. 4(b) appearing at $k = \pm \frac{\pi}{2}$ are near 1.5 meV and 1.35 meV in States 7 and 8, respectively. In all other states, the error is all below 1.1 meV.

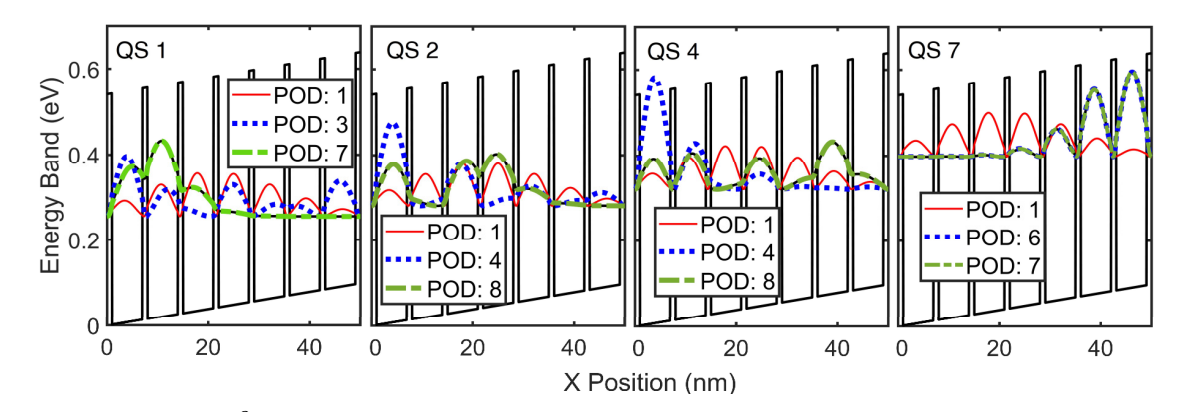


Figure 3. Profile of $|u_k|^2$ along x through its maximum in each of quantum states 1, 2, 4 and 7 in the QD structure at $k = \pi/2a$. POD-Galerkin predictions are compared to DNS results denoted by black lines (behind the green dashed lines).

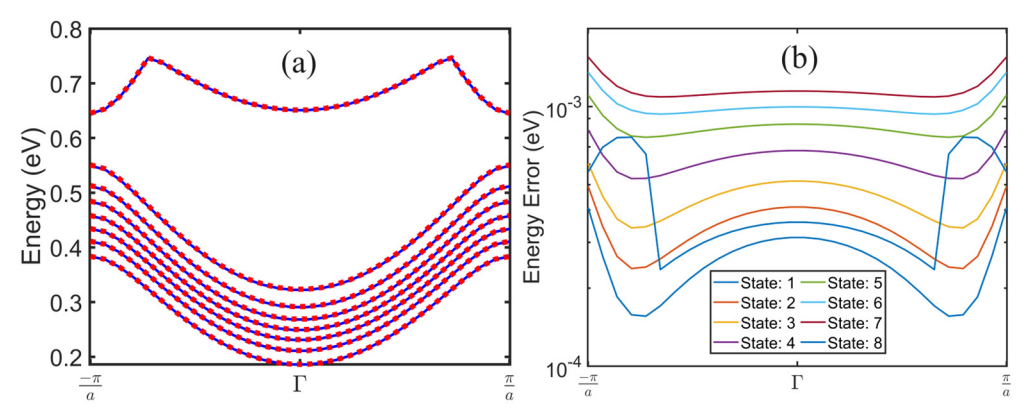


Figure 4. (a) Electronic band structure calculated from POD-Galerkin and DNSs. (b) Error of the band structure predicted by POD-Galerkin with respect to DNSs.

To examine the learning ability of POD-Galerkin beyond training, the demonstration is extended outside the training range below. Electric field at 35kV/cm is applied in simulations of the QD structure using the POD-Galerkin model trained by data generated by electric fields between 0 and 30 kV/cm in DNSs, as described above. As displayed in Fig. 5, all the WFs at $k = \pi/2a$ trained by the electric fields up to 30 kV/cm predicted by POD-Galerkin at 35kV/cm reach an *LSE* lower than 1.66% with 7 or 8 modes except for State 8 whose *LSE* is near 30% with 8 modes but reduces to 4.5%, 0.51% and 0.22 with 9, 10 or 11 modes, respectively. Similar to the interpolation case, WFs in States 1, 2, 6 and 7 predicted by POD-Galerkin are able to achieve an *LSE* near or below 1%. Even with a test field higher than the maximum training field, similar accuracy can be reached for State 1-7. For State 8 subjected to electric field beyond the training bounds, use of one more mode (10 modes instead of 9) than that for the State-8 WF in the interpolation case could reach similar accuracy (see

Fig. 2 compared to Fig. 5). Electronic ban structure calculated from POD-Galerkin and DNS are matched quite well for States 1 to 8 in the Brillouin zone, as shown in Fig. 6(a). The maximum error is near 1.45 meV observed in State 7, as shown in Fig. 6(b), and the next highest error is as small as 1.1 meV in State 6 at $k = \pm \frac{\pi}{a}$ even though the applied field is beyond the maximum training field. Such a learning ability for physics simulations beyond training is very difficult to achieve when using learning methods based on neural networks whose predictions beyond training are often unphysical.

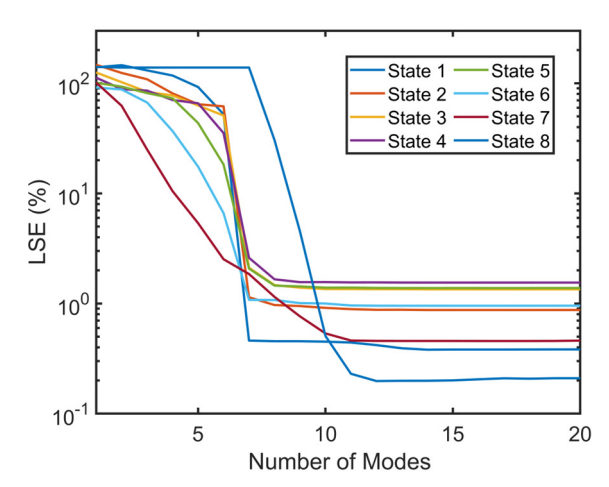


Figure 5. Relative *LSE* of POD-Galerkin with respect to the DNS results at $k = \pi/2a$ in the Brillouin zone at electric field of 35 kV/cm.

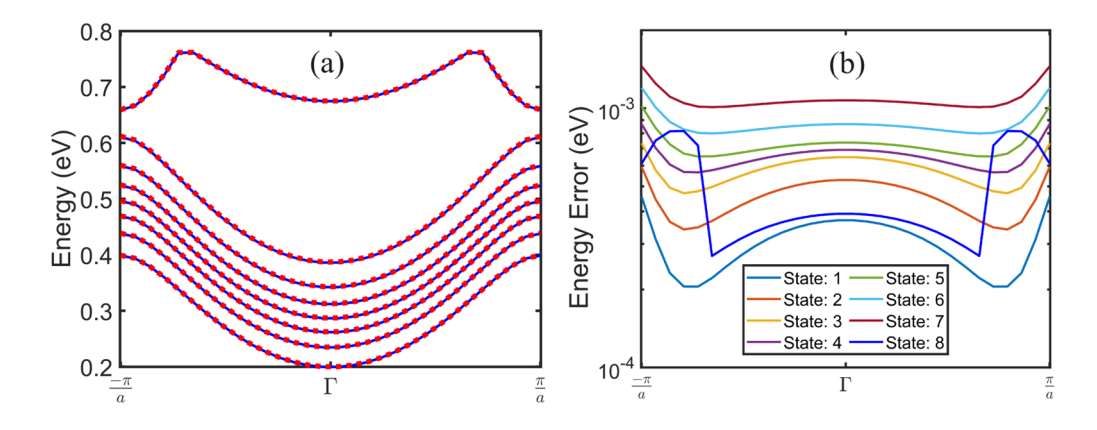


Figure 6. (a) Electronic band structure calculated from POD-Galerkin and DNSs. (b) Error of the band structure predicted by POD-Galerkin. Note that applied electrical field equals 35 kV/cm outside the range of training fields.

As discussed above, the complete solution of POD-Galerkin involves 2 steps. The matrix eigenvalue equation in (14) needs to be solved first in POD space for the eigenvector \mathbf{a} and eigenenergy $\mathcal{E}_{\mathbf{k}}$, which provides band structure (i.e., $\mathcal{E}_{\mathbf{k}}$ vs. \mathbf{k}) and takes little time. The second step however requires more time-consuming post processing in (7) using eigenvectors in POD space to find periodic spatial wave solution. For some applications that only require the electronic band structure, the computational speedup for POD-Galerkin in this demonstration is over 14,000 times compared to DNSs. When the WFs in space are also of interest, POD-Galerkin would enjoy an efficiency improvement of 150, 103 and 82 times for 5, 8 and 10 modes, respectively, over the DNSs.

3.2 Demonstrations in a 2D photonic crystal

The 2D photonic crystal structure is constructed by periodically repeated squares each of which consists of 4 discs with diagonally symmetrical refractive indices in the background with the refractive index n = 1, as shown in Fig. 7(a). DNSs of the structure are applied to solve the *TE*-mode wave equation given in (6) for $u_{\bf k}({\bf r})$ to collect the training data. In DNSs, periodic BCs are enforced in both directions, and 20 samples of refractive indices randomly generated between 2 and 4 with diagonal symmetry are implemented to collect training data. In each sample, the training data for the first 10 harmonic states are collected. There are thus 200 sets of data applied to generate one set of POD modes and eigenvalues for each ${\bf k}$ point in the 2D Brillouin zone. The first 65 eigenvalues in descending order are given in Fig. 7(b). The first 10 eigenvalues decline slowly and drop rapidly beyond 10th mode. The model parameters given by (20) and (21) are evaluated using the generated modes for the matrix eigenvalue equation in (19). With ${\bf a}$ solved from POD-Galerkin simulation of (19) in POD space for each ${\bf k}$ point, the optical band structure for the optical superlattice is evaluated in the Brillouin zone and post processing using (7) is performed to find periodic electric field $u_{\bf k}({\bf r})$.

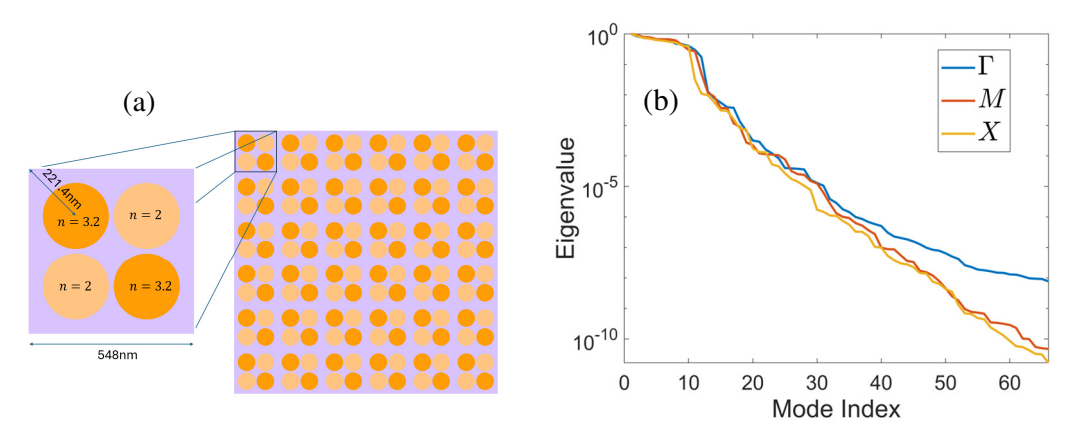


Figure 7. (a) 2D photonic crystal. (b) POD eigenvalues in descending order at the Γ , M and X points in the Brillouin zone.

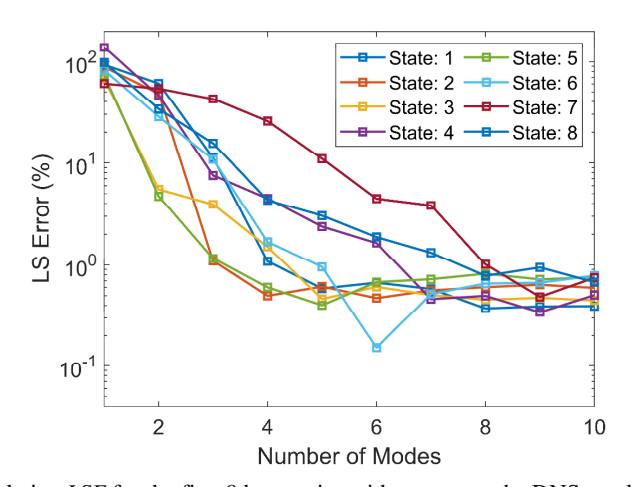


Figure 8. Relative LSE for the first 8 harmonics with respect to the DNS results at the M point.

For the first demonstration, the diagonal refractive indices of 2 and 3.2, as given in Fig. 7(a), are implemented in POD-Galerkin and DNSs of the 2D photonic crystal. As illustrated in Fig. 8 for the LSE derived from POD-Galerkin at the M point of the Brillouin zone, the periodic wave solutions $u_k(\mathbf{r})$ in all harmonic states derived from POD-Galerkin achieve reach an LSE below 3%, 1.9% or 1.32% with just 5, 6 or 7 modes, respectively, except for State 7. The LSE for State 7 is near 11%, 4.46% or 3.83% with 5, 6 or 7 modes, respectively. The LSE of the POD-Galerkin prediction for electric field waves in many states (such as 1,2, 3, 5 and 6) is below 1% with just 5 modes. When using 8 or more modes, they all drop near or below 1%. The profiles of $|u_k|^2$ at the M point in both x and y directions through the maximum $|u_k|^2$ are also

included in Fig. 9 for Harmonic States 1, 4, 7 and 8. The $|u_k|^2$ profiles between POD-Galerkin and DNSs agree very well using just 5 modes for States 1, 4 and 8 and 8 modes for State 7. Fig. 10 also illustrates an excellent agreement between the optical band structure predicted by POD-Galerkin and DNS. Their results overlap nearly perfectly with larger deviations near the M point. Errors at the M point for all 8 harmonic frequencies included in Fig. 10 are all below 0.048%.

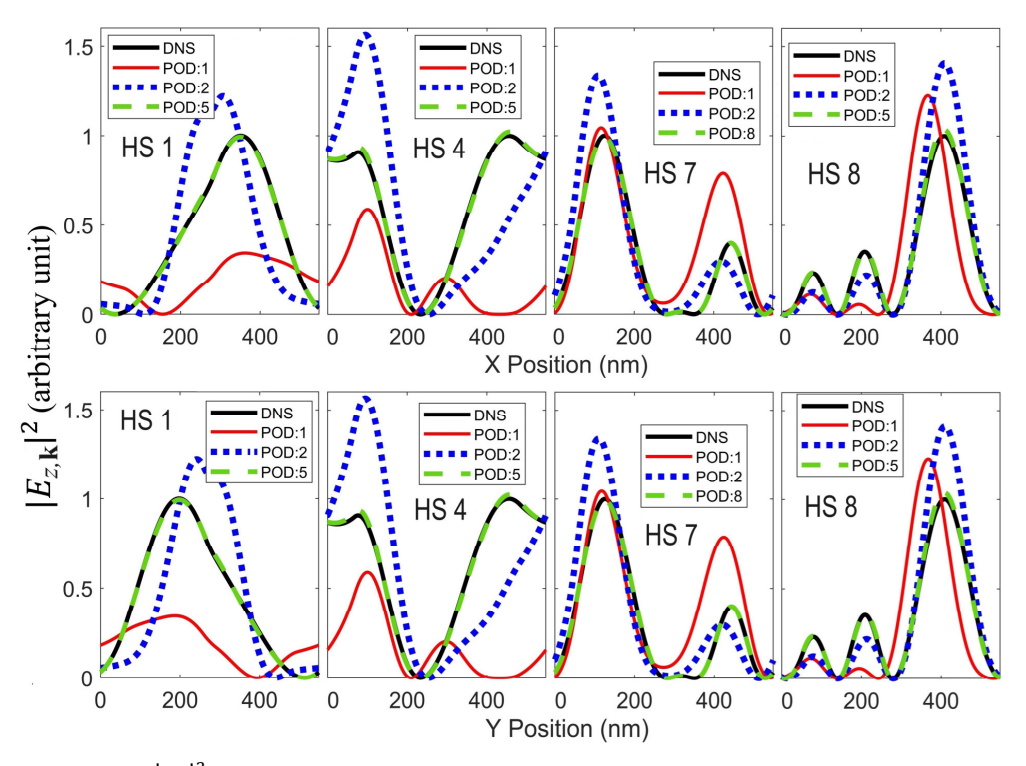


Figure 9. (a) Profiles of $|u_{\mathbf{k}}|^2$ in Harmonic States 1, 4, 7 and 8 in x and y directions through the peaks. Results predicted by POD-Galerkin are compared to those from DNSs denoted by black solid lines.

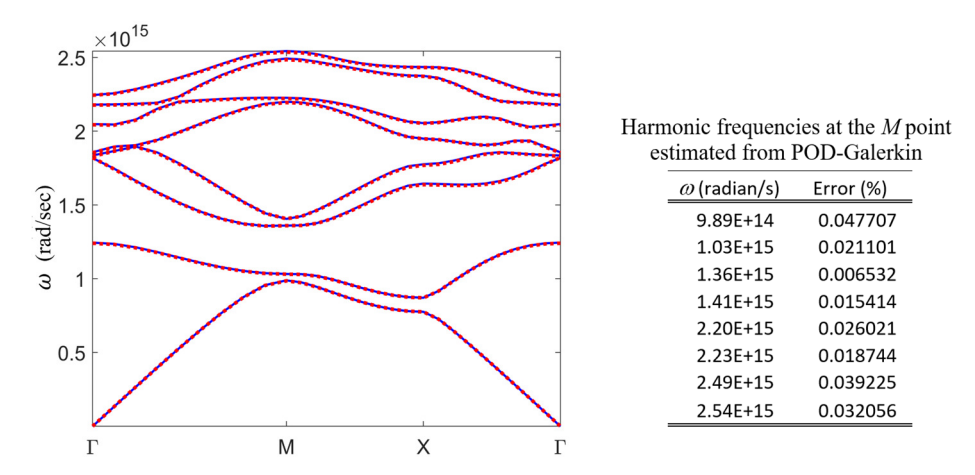


Figure 10. Electromagnetic band structure calculated from POD-Galerkin and DNSs. The table includes the 8 harmonic frequencies and their errors at the *M* point predicted by POD-Galerkin.

The second demonstration in the photonic crystal includes a refractive index outside the training bounds. The index n = 3.2 for the 2 diagonal discs in the photonic crystal given in Fig. 7(a) is replaced by n = 5 that is beyond the maximum refractive index of 4 used in training data collection. For the other 2 discs, the index remains unchanged. As illustrated in

Fig. 11, the *LSE* induced by POD-Galerkin at the *M* point for electric field wave solutions in all harmonic states is only slightly larger except for higher States 7 and 8. However, more modes can be included to offer a prediction with similar accuracy for States 7 and 8. For example, an LSE below 1.2% can be achieved for States 1-6 when using 6 modes. However, 15 or 11 modes are needed for States 7 or 8 to reach an *LSE* near 1.18% or 1.05%, respectively in this extrapolation case while only 8 modes are needed in the interpolation case. Fig. 12 also includes the optical band structure predicted by POD-Galerkin that matches DNS results nearly perfectly even in this extrapolation case. The errors at the *M* point for all 8 harmonic frequencies are all below 0.043%, as given in Fig. 12.

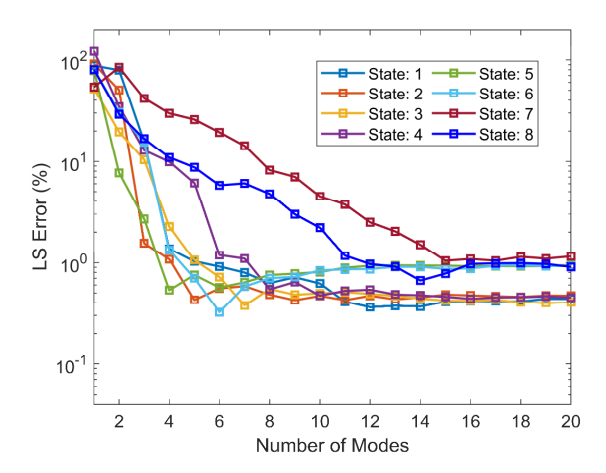


Figure 11. Relative *LSE* for the first 8 harmonic states resulting from POD-Galerkin at the *M* point in the Brillouin zone. Note that the refractive index in two of the diagonal discs is outside the training bounds.

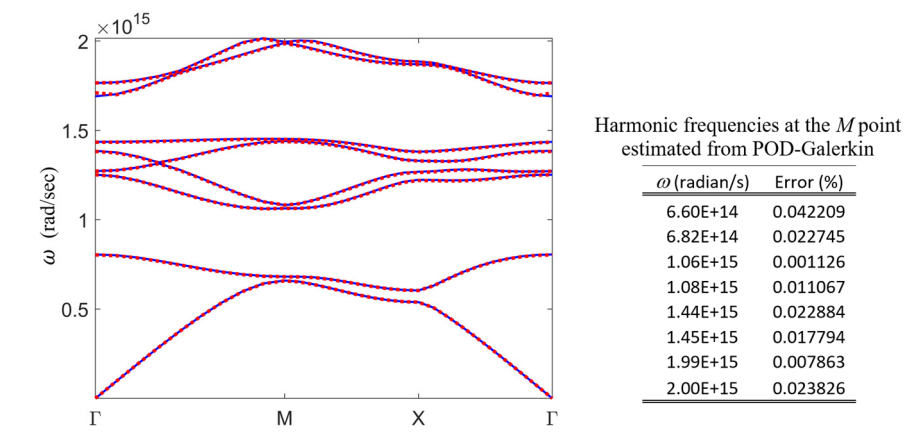


Figure 12. Electromagnetic band structure calculated from POD-Galerkin and DNSs. The table includes the 8 harmonic frequencies and their errors in percentage at the *M* point predicted by POD-Galerkin. Note that the refractive index in two of the diagonal discs is outside the training bounds.

Similar to the periodic nanostructure, the computation time for the eigen solution from (19) in POD space for the 2D photonic crystal is considerably shorter than post processing in (7) to evaluate the spatial wave solution. If one only needs the band structure, POD-Galerkin offers a reduction in computational time by 15,000 times compared to DNSs. When the electric field wave solution is also needed via post processing in (7), computing efficiency for POD-Galerkin over DNSs would be improved by 200 and 110 times for 5 and 8, respectively.

4. CONCLUSIONS

An effective and accurate physics-informed learning methodology has been presented and applied to predict wave solutions and band structures in electronic and optical periodic structures. The simulation methodology is derived from POD with the Galerkin projection of the wave equation to close the system. The POD generates basis functions (or POD modes) via solution data collected from DNSs subjected to parametric variations of the system including the BCs. The generated modes are optimized and tailored to the parametric variations of the system. The Galerkin projection then implements physical principles during simulation to further enhance the accuracy and efficiency of the approach. The physical principles enforced by the Galerkin projection offer a remarkable learning ability for POD-Galerkin to efficiently predict wave solutions and band structures outside the training bounds with very good accuracy. It has been demonstrated that the POD-Galerkin simulation methodology performs accurate simulations of 2D periodic quantum nanostructure and photonic crystals and renders a reduction in DoF by nearly 4 orders of magnitude, compared to DNSs. As a result, a computing speedup near 15,000 times over the DNSs can be achieved with extremely high accuracy for both electronic and optical periodic structures if only band structure calculations are of interested without the wave solution. If both wave function solution and band structure are required, a reduction in computational time near 2 orders of magnitude can be achieved with an LSE near 1%. In situations where the training was incomplete or the eigenstates are slightly beyond the training bounds, high accuracy with an LSE near 1%-2% can still be achieved if more POD modes are included.

ACKNOWLEDGEMENTS

This study is partially supported by the National Science Foundation under Grant No. OAC-2244049.

REFERENCES

- [1] E. Ozbay, I. Bulu, K. Aydin, H. Caglayan, K. Guven, "Physics and applications of photonic crystals," Photonics and Nanostructures Fundamentals and Applications, 2(2), 87-95 (2004). https://doi.org/10.1016/j.photonics.2004.08.001
- [2] G.-J. Tang, X.-T. He, F.-L. Shi, J.-W. Liu, X.-D. Chen, J.-W. Dong, "Topological Photonic Crystals: Physics, Designs, and Applications," Laser & Photonics Reviews, 16, 2100300 (2022). https://doi.org/10.1002/lpor.202100300
- [3] U. Biswas, C. Nayak, J. K. Rakshit, "Fabrication techniques and applications of two-dimensional photonic crystal: history and the present status," Optical engineering, 62(1), 010901-010901 (2023).
- [4] J. Zhuang, et. al., "Band Gap Modulated by Electronic Superlattice in Blue Phosphorene," ACS Nano, 12 (5), 5059-5065 (2018).
- [5] Y. Zhang, Y. Kim, M. J. Gilbert, et al., "Electronic transport in a two-dimensional superlattice engineered via self-assembled nanostructures," npj 2D Mater Appl, 2, 31 (2018).
- [6] R. B. Hwang, "A theoretical design of evanescent wave biosensors based on gate-controlled graphene surface plasmon resonance," Sci Rep, 11, 1999 (2021).
- [7] K. Busch, G. von Freymann, S. Linden, S.F. Mingaleev, L. Tkeshelashvili, M. Wegener, "Periodic nanostructures for photonics," Physics Reports, 444, 101-202 (2007). https://doi.org/10.1016/j.physrep.2007.02.011.
- [8] P. Pereyra, "Advances in the calculation of optical properties in superlattices; novel insights derived from the theory of finite periodic systems," Annals of Physics, 397, 159-191 (2018).
- [9] R. B. Hwang, "Periodic structures: mode-matching approach and applications in electromagnetic engineering," John Wiley & Sons (2012).
- [10] H. Oraizi, M. Afsahi, "Analysis of planar dielectric multilayers as FSS by transmission line transfer matrix method (TLTMM)," Prog. in Electromagnetics Res. 74, 217-240 (2007)
- [11] H. H. Tung, C. P. Lee, "An energy band-pass filter using superlattice structures," IEEE J. Quantum Electronics 32(3) 507-512 (1996).
- [12] Y. Wang, "Transfer matrix theory of monolayer graphene/bilayer graphene heterostructure superlattice," J. Appl. Physics 116, 164317 (2014).
- [13] L. R. Ram-Mohan, K. H. Yoo, R. L. Aggarwal, "Transfer-matrix algorithm for the calculation of the band structure of semiconductor superlattices," Physical Rev. B 38(9) 6151 (1988).
- [14] M. Veresko, M. C. Cheng, "Physics-informed Reduced-Order Learning from the First Principles for Simulation of Quantum Nanostructures," Scientific Reports, 13 6197 (2023).

- [15] J. L. Lumley, "The structure of inhomogeneous turbulence, Atmospheric Turbulence and Wave Propagation," A. M. Yaglom and V. I. Tatarski, Eds. Moscow, Russia: Nauka, 166–178 (1967).
- [16] L. Jiang, A. Dowling, M. C., Cheng, Y. Liu, "PODTherm-GP: A Physics-Based Data-Driven Approach for Effective Architecture-Level Thermal Simulation of Multi-Core CPUs," IEEE Trans. Computers, 72(10) 2951-2962 (2023).
- [17] W. Jia, B. T. Helenbrook M. C. Cheng, "Fast Thermal Simulation of FinFET Circuits Based on a Multiblock Reduced-Order Model," IEEE Trans. CAD of ICs & Sys., 35 (7), 1114-1124 (2016). doi: 10.1109/TCAD.2015.2501305
- [18] M. Cheng, "A Reduced-Order Presentation of the Schrödinger Equation," AIP Advances 6(9) 095121 (2016).
- [19] L. Jiang, Y. Liu, M. C. Cheng, "Predicting Hot Spots in a Ten-Thousand-Core GPU with a 5-Order Speedup over FEM Enabled by a Physics-based Learning Algorithm," 2024 InterSociety Conf. Thermal and Thermomechanical Phenomena in Electronic Systems (ITherm 2024), May 28-May 31 (2024).
- [20] M. Rasht-Behesht, C. Huber, K. Shukla, G. F. Karniadakis, "Physics-informed neural networks (PINNs) for wave propagation and full waveform inversions," J. Geophysical Research: Solid Earth, 127, e2021JB023120 (2022). https://doi.org/10.1029/2021JB023120
- [21] S. Cai, Z. Mao, Z. Wang, et al. Physics-informed neural networks (PINNs) for fluid mechanics: a review. Acta Mech. Sin. 37, 1727–1738 (2021). https://doi.org/10.1007/s10409-021-01148-1
- [22] B. Moseley, A. Markham, T. Nissen-Meyer, "Finite basis physics-informed neural networks (FBPINNs): a scalable domain decomposition approach for solving differential equations," Adv Comput Math 49, 62 (2023). https://doi.org/10.1007/s10444-023-10065-9
- [23] Sirovich, L.: Turbulence and the dynamics of coherent structures. I. Coherent structures, Quart. Appl. Math. 45(3) 561–571 (1987).
- [24] W. Jia, M. C. Cheng, "A methodology for thermal simulation of interconnects enabled by model reduction with material property variation," J. Computational Sci. 61, 101665 (2022).